Low-energy electron microscopy of CO/Pt(111) surface diffusion by nonequilibrium coverage profile evolution

C. M. Yim,[1] K. L. Man,[1] Xudong Xiao,[1,2] and M. S. Altman[1,*]
[1]*Department of Physics, The Hong Kong University of Science and Technology, Clear Water Bay, Kowloon, Hong Kong*
[2]*Department of Physics, The Chinese University of Hong Kong, Shatin, New Territories, Hong Kong*
(Received 11 April 2008; revised manuscript received 24 September 2008; published 30 October 2008)

The adsorption and diffusion of CO molecules on a Pt(111) surface have been studied using low-energy electron microscopy (LEEM). The explicit relationship between LEEM image intensity and CO coverage that is determined during adsorption is used to characterize nonequilibrium CO coverage profiles that are subsequently prepared by laser-induced thermal desorption. Real-time observations of the temporal evolution of these profiles toward equilibrium uniform coverage distributions are analyzed by predictive and inverse solutions of the diffusion equation. These two methods determine consistently the detrimental effect on diffusion of the laser-induced surface damage that is observed directly with LEEM. The inverse method also provides independent information on the coverage dependence of diffusion with high coverage resolution.

DOI: 10.1103/PhysRevB.78.155439 PACS number(s): 68.43.Jk, 68.37.Nq, 68.47.De, 02.30.Zz

I. INTRODUCTION

Many physical and chemical processes at surfaces involve significant mass transport of atoms or molecules. This may produce nonequilibrium arrangements of the participating species that are uniquely defined by the nature of diffusion and other relevant mediating kinetic processes. Access to direct information on adatom or admolecule coverage profiles during nonequilibrium phenomena would therefore provide means for testing basic assumptions that are made in our understanding of these phenomena.

Due to its fundamental importance, surface diffusion is one of the longest studied problems in surface science.[1] Over the years, many experimental methods have been developed for studying surface diffusion. A substantial number of these examine the evolution of nonequilibrium coverage profiles toward equilibrium uniform distribution. One method that is frequently used to prepare nonequilibrium coverage profiles is laser-induced thermal desorption (LITD). Many approaches have been taken to monitor profile evolution following LITD including hole refilling methods,[2–11] linear optical diffraction (LOD),[12–15] and photoemission electron microscopy (PEEM).[16–18] Low-energy electron microscopy (LEEM) has also been used to study surface diffusion indirectly by observing how some features at a surface change in response to mass transport under nonequilibrium conditions, e.g., step motion during island coarsening or growth,[19,20] domain evolution,[21] etc.

It is known that the adsorption of gasses on surfaces can have a dramatic effect on the elastically reflected electron intensity at very low incident energy.[22] This means that there is significant potential for measuring coverage profiles directly with high lateral resolution using LEEM. The purpose of this work is to characterize the sensitivity of LEEM to variations in gas coverage and then to exploit this sensitivity to study diffusion by observing nonequilibrium coverage profile evolution directly with LEEM following LITD. One potential advantage of this approach is that it may allow for the study of surface diffusion with high spatial resolution. It can also provide complementary information on surface structure and morphology that is typically accessible to LEEM. This additional information may prove to be valuable for interpreting surface diffusion results. The system we have investigated is CO on the Pt(111) surface. The adsorption, desorption,[23–28] and diffusion[6,13–15,28–32] of CO on Pt(111) have been studied extensively in the past.

II. EXPERIMENTAL RESULTS

A. Experimental details

The experiments were carried out in a low-energy electron microscope with a base pressure of 5×10^{-11} torr. The imaging principle, contrast mechanisms, and real-time imaging capability of LEEM have been described previously.[33,34] The Pt surface was oriented to within 0.1° of the (111) orientation. It was cleaned by repeated cycles of Ar ion sputtering at 1.5 kV at 300 K followed by annealing to 1300 K to remove sputter damage. It was then annealed at 1100 K in an oxygen pressure of 1×10^{-7} torr oxygen to remove carbon impurities, as necessary. These standard procedures produced a (1×1) LEED pattern with sharp diffraction spots and uniform terraces in LEEM images without step pinning due to impurities.

LITD was carried out using a pulsed Nd:YAG laser ($\lambda=1064$ nm). The laser was operated in Q-switch mode with pulse width of 8–10 ns. In our optical setup, the path length was set to be approximately 4 m, in order that higher-order modes, which have larger spatial extent than the TEM_{00} mode, could be separated out. Then, the temporal and spatial distributions are approximately Gaussian because of the dominating 00 mode. A $\lambda/2$ plate and a thin-film polarizer were inserted into the optical path in order to obtain fine control over the incident laser power. The energy of a single laser pulse that was used to desorb CO from Pt(111) at 300 K in this work is estimated to be 0.4 mJ. This estimate is based on a power measurement that was performed outside of the vacuum chamber at a position in front of the focusing lens and a deflecting mirror.

The laser beam was inserted into the LEEM through a window that is located opposite to the sample. From there,

the beam passed along the electron-optical axis of the microscope objective lens and through a small hole in the objective before striking the sample at normal incidence. The incident electron beam also passes through the same hole in the objective lens. The impact position of the laser beam on the sample was adjusted to overlap the electron beam, such that the LITD region was located in the LEEM image field of view. However, the insertion window is disadvantageously located a distance of almost 40 cm from the sample surface. This long distance is detrimental for focusing the laser beam to a small spot size at the sample. The diffraction limited spot size full width at half maximum (FWHM) was calculated to be on the order of 50–100 μm. CO desorbs from the central area of the spot where the incident energy exceeds the desorption threshold. The laser-pulse energy could be controlled to produce desorption regions with FWHM on the order of 25 μm, which could be suitably imaged by operating the LEEM with a 100 μm image field of view.

B. Detecting CO coverage variations using LEEM

In order to characterize CO coverage profiles quantitatively using LEEM, it is necessary to have prior detailed knowledge of the relationship between LEEM image intensity and CO coverage. From the point of view of optimizing the coverage resolution of the measurement, we must also identify the imaging electron energy that provides the greatest sensitivity to CO coverage. The optimum imaging energy was determined by measuring LEEM image intensity versus energy, or LEEM $I(V)$ curves, repeatedly during exposure of the Pt(111) surface to CO until saturation. The exposure was carried out at a CO pressure of $P_{CO}=2.2\times10^{-9}$ torr at room temperature, which leads to saturation at close to 0.5 monolayer (ML) coverage.[23–27] The measurements focused on the energy range of 2–30 eV, where the reflected electron intensity and signal-to-noise ratio are generally high. The results of these measurements are shown in Fig. 1(a). The predominant effect that can be seen in this figure is that a prominent Bragg peak in the $I(V)$ curve of the clean surface decreases monotonically during CO exposure. The energy dependence of this reflectivity change is revealed more clearly by dividing the LEEM $I(V)$ curve of the clean surface by $I(V)$ curves for the CO exposed surface at later times. The peak in the resulting ratio curves, shown in Fig. 1(b), indicates that CO adsorption has the greatest effect on the reflected intensity at an incident energy of $E=15.6$ eV. At this energy, the LEEM image intensity changes by a factor of over 30 times between the clean surface and the CO-saturated surface. If this change is spread over the 4000+ intensity levels of the 12-bit CCD camera that is used in these experiments, then LEEM is sensitive ideally to CO coverage variations on the order of about 1×10^{-4} ML on average. This estimate assumes a linear relationship between CO coverage and LEEM intensity over the entire coverage range to saturation. The sensitivity that is actually achieved in the experiment differs because of the nonlinear relationship between intensity and coverage. In particular, the intensity change caused by CO adsorption saturates already as the coverage reaches about 0.35 ML. At lower CO coverage, LEEM is highly sensitive to changes in CO coverage. At higher coverage, LEEM is insensitive to changes of CO coverage. Although the coverage resolution will also be degraded, in practice, by image noise, this does not appear to be a serious problem in the present investigations.

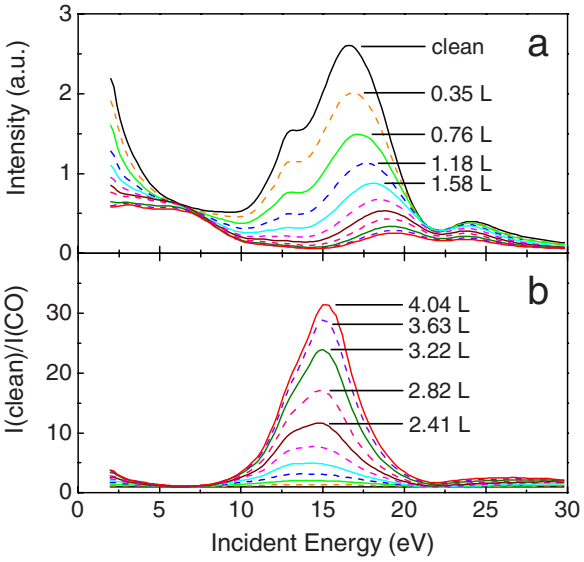

FIG. 1. (Color online) (a) LEEM image intensity vs incident electron energy, $I(V)$, curves measured consecutively during continuous exposure of the Pt(111) surface to CO. The accumulated exposure during the measurement of each individual curve was approximately 0.4 L. (b) The ratios of the $I(V)$ curve for the clean surface to the curves for the CO exposed surface in (a) exhibit a peak that identifies the optimal imaging energy for detecting CO.

More detailed measurements of the reflected intensity variation caused by CO adsorption were then carried out at the optimum imaging energy at the same CO partial pressure and sample temperature. The intensity that is measured continuously at 15.6 eV imaging energy during CO exposure is shown in Fig. 2(a). This result agrees well with the discrete intensity change at 15.6 eV, shown as symbols in Fig. 2(a), which is obtained from the consecutive $I(V)$ curves in Fig. 1(a). The exposure dependence shown in Fig. 2(a) is converted to coverage dependence in Fig. 3 using empirical results for site-dependent CO coverage versus exposure that were obtained previously with electron energy-loss spectroscopy (EELS) (Fig. 2 in Ref. 24). The previous EELS results that we use for this conversion, which are reproduced schematically in Fig. 2(c), were obtained under conditions of dosing pressure and sample temperature that were very similar to those used here. We note that the LEEM intensity change shown in Fig. 3 saturates considerably earlier than the total CO coverage reaches saturation.

CO adsorption is also known to modify the Pt(111) work function.[25] Therefore, measurements of the concurrent work-function change $\Delta\phi$ can provide an important test of the foregoing results for the intensity variation. The work-function change caused by CO adsorption was probed by monitoring the onset of the mirror imaging mode in LEEM. In mirror mode, the incident electron kinetic energy is too low to overcome the decelerating potential in the objective lens near the sample surface. Consequently, the electron

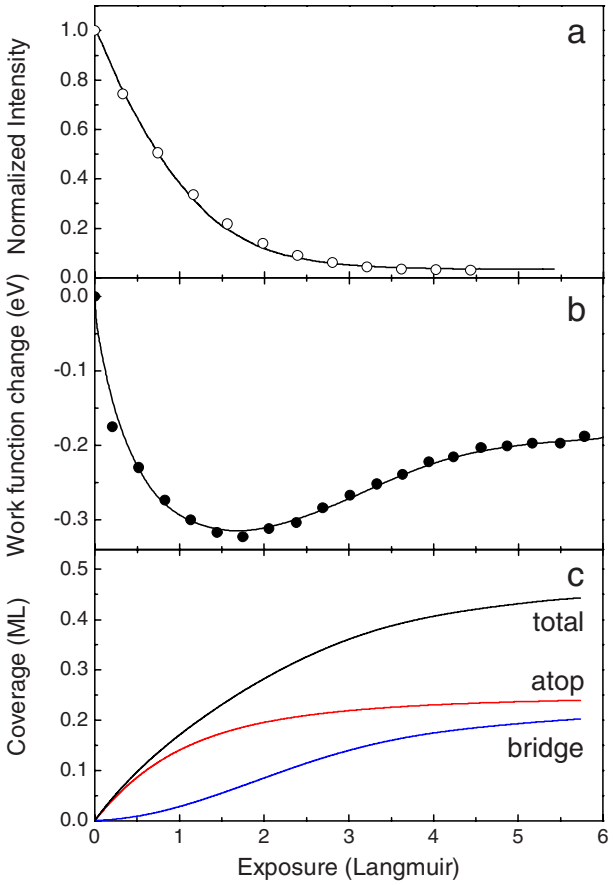

FIG. 2. (Color online) (a) The continuous variation in the LEEM image intensity at 15.6 eV during CO exposure normalized to the initial intensity for the clean surface is indicated by the solid line. The open symbols (○) are the discrete values of the normalized intensities at 15.6 eV obtained from the $I(V)$ curves shown in Fig. 1(a). (b) The work-function change during CO exposure of the Pt(111) surface is indicated by solid symbols (●). The solid line is a polynomial fit that has no significance other than to highlight the trend. (c) The site-dependent and total coverage vs CO exposure taken from Ref. 24.

beam is completely reflected at an equipotential plane in front of the surface. The transition from conventional LEEM imaging mode to mirror mode occurs when the incident electron energy is lowered sufficiently. This produces an increase in the reflected intensity to unity. For Pt(111) and many other metal surfaces, this transition usually falls in the energy range $-0.5 < E < 1.5$ eV (Fig. 4). The onset of mirror mode is identified by the inflection point of the $I(V)$ curve during this transition. In LEEM, the incident electron energy is defined by the voltage bias between the electron gun cathode and the sample, with a constant offset that is produced by the work-function difference between cathode and sample. During CO exposure of the sample surface, the work function of the cathode, which is isolated from the CO, is unaffected. Therefore, any shift of the inflection point during CO exposure can only be due to a change in the sample work function.

The slope of the $I(V)$ curve at the inflection point, which determines the sensitivity of the work-function change measurement, is influenced by the energy spread of the incident electron beam and by the shape of the surface-barrier potential. The results presented below indicate that the work-function change can be measured with good resolution by this method for typical surface-potential barrier and energy

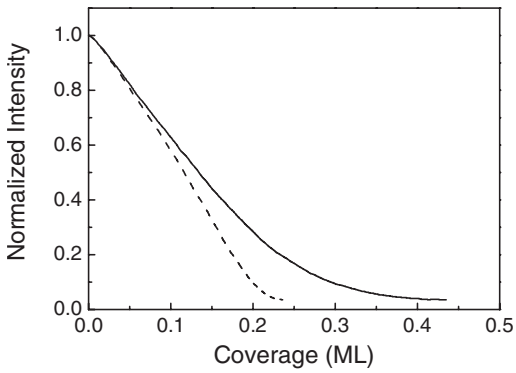

FIG. 3. The dependence of the normalized LEEM intensity on total CO coverage on the Pt(111) surface is indicated by the solid curve. Attributing the intensity change to atop site coverage only produces the dashed curve. The normalization is with respect to the intensity for the clean surface.

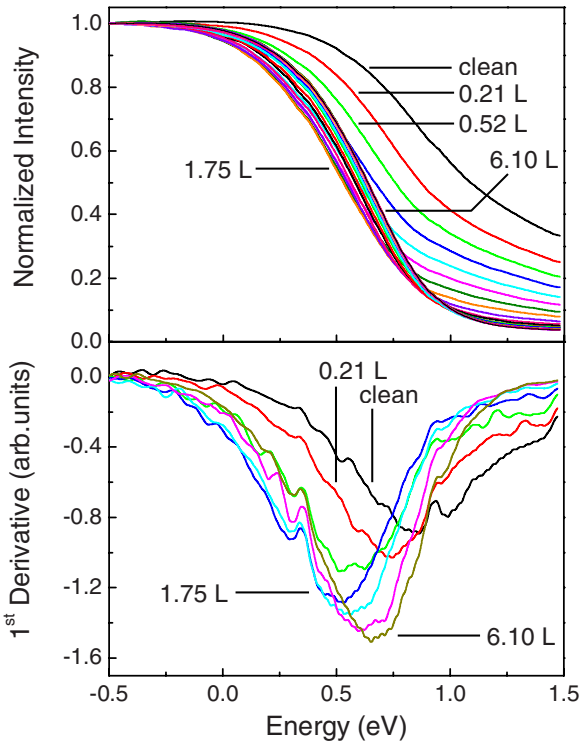

FIG. 4. (Color online) (a) LEEM $I(V)$ curves at the onset of mirror mode were measured consecutively during continuous exposure of the Pt(111) surface to CO. Following the measurement at 0.21 L, the exposure increment is approximately 0.3 L. The energy scale refers to the voltage bias between sample and electron gun cathode. The curves corresponding to the work-function minimum (1.75 L), the initial three (clean, 0.21 L and 0.52 L), and the final (6.1 L) exposures in this set are indicated. (b) First derivatives of selected $I(V)$ curves in (a) for the clean surface and exposures of 0.21, 0.52, 0.83, 1.75, 2.38, 3.33, and 6.10 L.

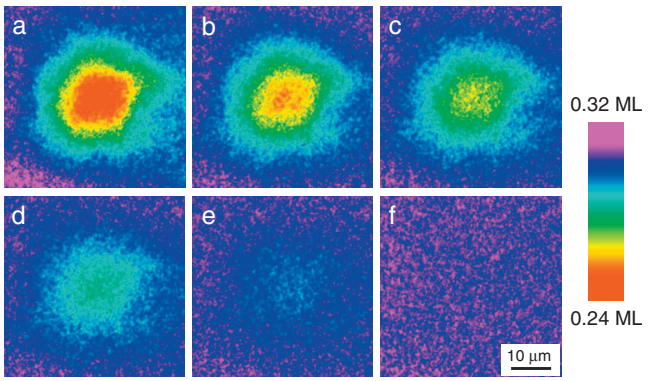

FIG. 5. (Color) LEEM images show the temporal evolution at 300 K of a nonequilibrium coverage profile of CO on Pt(111) at (a) $t=0$ (immediately after LITD), (b) 6.7, (c) 13.5, (d) 27.5, (e) 55, and (f) 110 s.

spread. The exposure resolution of the measurement is optimized, subject to signal-to-noise considerations, by using low gas exposure pressure and high $I(V)$ curve scanning rate. The $I(V)$ curve scanning rate is given by the energy window and the size of the energy step which are 2.0 and 0.02 eV, respectively, here. The use of a larger energy step will have a detrimental effect on the energy resolution of the work-function change measurement.

The data in Fig. 4(a) that show the transition to mirror mode were obtained at a CO pressure of $P_{CO}=2.2\times10^{-9}$ torr at room temperature, same as the measurements of CO adsorption shown in Figs. 1 and 2(a). The location of the inflection point is easily discerned by the peak in the first derivative shown in Fig. 4(b). The work-function change that is determined by tracking the peak in the first derivative during CO exposure is shown in Fig. 2(b). This result is in good qualitative agreement with the earlier results.[25] We find that the work function reaches a minimum at an exposure that corresponds to a total coverage of 0.25 ML according to the EELS results. It also saturates as the exposure approaches 6 langmuir (L), in agreement with the coverage saturation observed by EELS [Fig. 2(c)].

The work-function result shown in Fig. 2(b) confirms that the CO coverage saturates well after the LEEM intensity does. The EELS data also indicate that the filling of the bridge sites lags behind the atop site filling. These observations suggest that the LEEM intensity variation is possibly more sensitive to atop site occupation than to bridge site occupation. If we assume the extreme case that the electron scattering is sensitive only to the occupation of atop sites, then the intensity variation versus atop site coverage indicated by the dashed curve in Fig. 3 is obtained. In practice, we will use the empirical intensity vs total coverage relationship (solid curve in Fig. 3) to interpret LEEM intensity during profile evolution. This treatment assumes that local equilibrium between atop and bridge site occupation is maintained during mass transport.

C. Profile evolution measurements and analysis

CO diffusion on the Pt(111) surface was studied by observing the temporal evolution of nonequilibrium coverage profiles toward equilibrium with LEEM. Nonequilibrium profiles were prepared by exposing the surface first to a prescribed amount of CO and then illuminating the CO-covered surface with a single Nd:YAG laser pulse. An example of a CO coverage profile immediately following LITD and at a few times during its temporal evolution is shown in Fig. 5. Coverage in Fig. 5 was determined from raw image intensity using the empirical relationship shown in Fig. 3. The initial CO coverage before desorption was slightly more than 0.31 ML and the maximum amount of CO that was desorbed from the middle of the desorption region is just over 0.06 ML in Fig. 5. The LEEM imaging rate was 1.8 frames/s in these experiments. Although the images provide detailed information on the two-dimensional profile evolution, we take advantage of the nearly circular symmetry depicted in Fig. 5 to simplify this problem at the outset by treating it in terms of the radial coordinate only. Radial coverage line profiles originating from the center of the desorption region are measured in each image with 1° azimuthal angle interval. These are then combined to produce an average radial coverage profile shown in Fig. 6 at several times following LITD. The

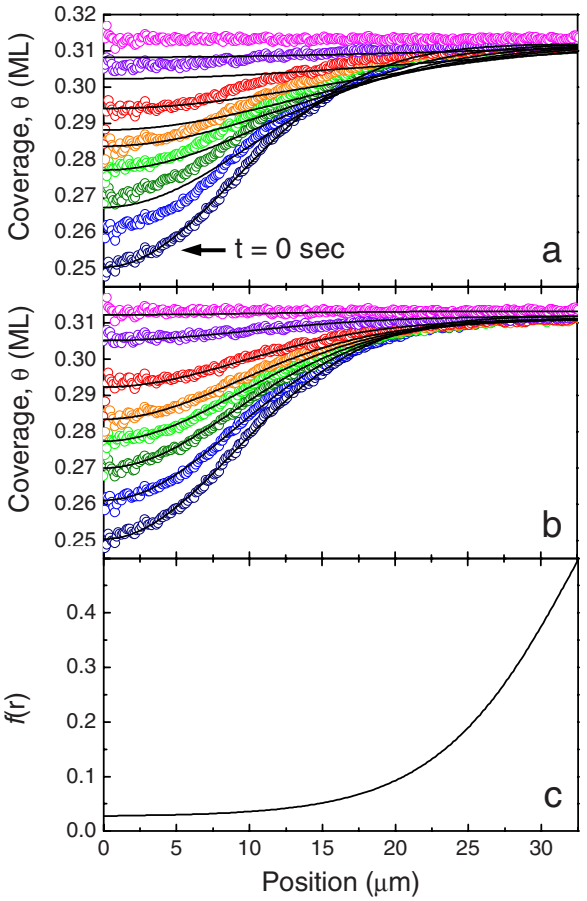

FIG. 6. (Color online) Radial line scans of CO concentration profiles during profile evolution are shown in comparison with the best-fit solutions of the diffusion equation (solid lines) at times $t=0$, 5.5, 11, 16.5, 22, 33, 66, and 132 s (from bottom to top) for (a) coverage-dependent diffusion coefficient and (b) position and coverage-dependent diffusion coefficient. The optimized spatial component of the diffusion coefficient $f(r)$ used to fit the data in (b) is shown in (c).

solid line through the initial profile at $t=0$ is a fit of a Gaussian function.

1. Analysis I: Predictive solution the diffusion equation

The first approach to extracting information about diffusion from the experimental data is to model profile evolution by numerical solution of the diffusion equation. The general idea of this approach is to predict the correct (experimentally observed) evolution from a known initial condition and subject to known boundary conditions by appropriate selection of control parameters (the diffusion coefficient here) in the governing diffusion equation. The success of this approach depends crucially on the validity of the governing equation that is used. It also requires that the functional forms of the control parameters are anticipated correctly.

We begin with the general form of the diffusion equation for circular symmetry

$$\frac{\partial \theta}{\partial t} = \frac{1}{r}\frac{\partial}{\partial r}\left(rD\frac{\partial \theta}{\partial r}\right) + J \cdot S(\theta) - \frac{\theta}{\tau}, \tag{1}$$

where D is the diffusion coefficient, θ is the coverage, J is an incident flux due to residual gas, $S(\theta)$ is the coverage-dependent sticking coefficient, and τ is the desorption lifetime. The incident flux is related to the partial pressure of CO P according to $J=P/\sqrt{2\pi mkT}$, where m is the molecular mass, k is Boltzmann constant, and T is temperature. The desorption lifetime is equal to the inverse of the desorption rate $\tau=[\nu \exp(-E_d/kT)]^{-1}$, where ν is the attempt frequency and E_d is the desorption activation energy. We use $\nu=4\times10^{15}$ s^{-1} and coverage-dependent desorption energy $E_d=(1.44-0.75\theta)$ eV that were determined previously.[23] Nearly identical results are obtained in our analysis using very similar desorption parameters $E_d=[(1.43\pm0.1)-(0.65\pm0.09)\theta]$ eV and $\nu=1.2\times10^{(15\pm1)}$ s^{-1} that were determined more recently by a site-dependent modeling scheme.[26] Although this modeling also provides detailed information about sticking coefficient,[27] we use a simplified expression given by Kisliuk[35]

$$S(\theta) = S_0\left(1+\frac{K\theta}{\theta_{\max}-\theta}\right)^{-1},$$

where $\theta_{\max}=0.5$ ML and model parameters $K=0.84$ and $S_0=0.3$ were determined previously for adsorption at 310 K and $P=9\times10^{-8}$ torr.[23] In fact, it turns out that the two terms relating to adsorption and desorption in Eq. (1) do not affect the results significantly in the present case due to dominant diffusion effects. They are included here for illustrative purposes.

The diffusion of CO on Pt(111) is known to be coverage dependent. Results that were obtained using the LOD technique quantify the coverage dependence approximately at room temperature in the relevant coverage range by the linear relationship $D(\theta)=D_0(A_0\theta+B_0)$, where $A_0=1.87$ and $B_0=-0.06$ and D_0 is a scale factor.[13] Although this expression is expected to be invalid as the coverage approaches zero, we apply it only in the vicinity of 0.3 ML where the present LEEM experiments were carried out. Very similar coverage dependence of the inverse lifetime of the time-dependent structure factor in ^{3}He spin-echo measurements was determined for collective motion of CO on Pt(111) in thermal equilibrium at 340 K.[28] Taking into account the coverage dependence of the diffusion coefficient, the appropriate form of the diffusion equation [Eq. (1)] is solved numerically by the finite difference method.[36] The Gaussian-fit profile at $t=0$ is taken as the initial condition, and a boundary is chosen that is greater than ten times the initial profile width. At that large distance, LITD is negligible and the change in boundary condition during the experiment is reasonably treated by the last two terms in Eq. (1) only. The change in coverage at the boundary between the baseline of the initial Gaussian profile and final uniform distribution fixes the residual CO partial pressure to the value of $P=1.1\times10^{-10}$ torr. The diffusivity scale factor D_0 is the only remaining adjustable parameter. The best fit of the model profile evolution, defined through the simultaneous fitting to the selected experimental profiles in Fig. 6(a), is obtained for $D_0=4.71\times10^{-8}$ cm^2/s.

It is evident that the model in its present form fails to describe profile evolution correctly. The predicted profiles obviously do not reproduce the experimental profile shapes faithfully and the predicted approach to equilibrium uniform distribution is too slow at late times. The model also predicts a characteristic spreading of the profile that is absent in the experimental data. In particular, the coverage is predicted to drop below the initial coverage at large radius $r>15$ μm due to the diffusive motion of molecules from the periphery to the core of the desorption region. Experimentally, this profile spreading effect is hardly observed. It has been shown that coverage-dependent diffusivity can suppress the spreading effect in modeling of nonequilibrium profile evolution.[37] However, the coverage dependence that was measured for Co/Pt(111) previously[13,28] has already been incorporated in the model to produce the ill-fitting model profiles in Fig. 6(a). Furthermore, we find that the discrepancy between model predictions and experimental profile evolution cannot be reduced significantly using a stronger coverage dependence in the present case.

An alternate mechanism that we consider is the possible influence of laser-induced surface damage. The evidence of damage obtained with LEEM is presented in Sec. II D. It is reasonable to expect that diffusivity is diminished due to damage and that the severity of damage is greater at the core of the desorption region than at its periphery. These two statements lead us to treat the diffusion coefficient as a spatially dependent quantity. We model profile evolution using a diffusion coefficient that has a circularly symmetric spatially (radial) dependent component described by the Boltzmann functional form

$$f(r) = \frac{\alpha-1}{1+\exp\left(\frac{r-r_c}{w}\right)} + 1, \tag{2}$$

where r_c is the radius that delineates the boundary between interior and exterior regions, w is the half width of the transition between these regions, and α is related to the fractional suppression of diffusion at the center. The complete form of the diffusion coefficient is then $D(r,\theta)=D_0f(r)(A_0\theta+B_0)$.

The appropriate form of the diffusion equation [Eq. (1)] with coverage- and radial-position-dependent diffusion coefficient is integrated numerically to model profile evolution. The best-fit result, shown in Fig. 6(b), is obtained with the following parameters: $D_0=9.12\times10^{-7}$ cm^2/s, $\alpha=2.68\times10^{-2}$, $r_c=32.8$ μm, and $w=4.9$ μm. The shape of the radial-dependent component $f(r)$ of the diffusion coefficient is shown in Fig. 6(c). Using this approach, the model fit to the experimental data in Fig. 6(b) is excellent.

2. Analysis II: Inverse parameter estimation

The second approach to extracting information about diffusion from the experimental data employs an inverse solution method. Inverse methods have been used in the past to determine thermal conductivity in heat conduction problems.[38,39] Since the governing equations for heat conduction and mass diffusion are the same, the inverse method is readily adapted to the present problem. Unlike the predictive modeling approach described above, in which the experimental profile evolution is replicated by guessing and adjusting the functional form and value of the diffusion coefficient, the diffusion coefficient is determined directly at every point in space and time from the data by the inverse method. Schematically, this is done by using the experimentally measured coverage in the neighborhood of a spatial position at one point in time to determine the local coverage gradients, $\partial\theta/\partial r$ in Eq. (1), and the measured coverage at that position at consecutive times to determine its time rate of change, $\partial\theta/\partial t$ in Eq. (1). This information is used to invert the diffusion equation and solve for the diffusion coefficient locally in space and time. The conservation of mass flowing between neighboring spatial positions in consecutive time steps imposes a constraint that produces a set of coupled equations, which are treated by the finite difference method.[36]

The inverse solutions are very sensitive to noise in the data. Therefore, we have used smooth Gaussian functions in the analysis that accurately represent the experimental coverage profiles at all times. We also use progressively longer time steps dt at later times that compensate to some extent for the diminishing coverage change as the profile gradually approaches equilibrium. In this way, the incremental coverage changes $d\theta$ that are used in the analysis are not exceedingly different at early and late times.

The values of the diffusion coefficient that are determined at different positions and at a few different times by this method are shown in Fig. 7(a). Although the spatial and coverage dependences are still intermingled in this result, the spatial dependence is dominant. Consequently, the result in Fig. 7(a) strongly resembles the spatial dependence that was inferred by the predictive method [Fig. 6(c)]. Assume that the spatial and coverage dependences are separable according to $D(r,\theta)=D_0f(r)g(\theta)$. Following this assumption, we extract the coverage dependence by examining the diffusion coefficient at different times during profile evolution (increasing coverage) at each position. Time is converted to coverage using the experimentally measured coverage at each position. The resulting coverage-dependent diffusion coefficient $D_0g(\theta)$ is shown in Fig. 7(c) for several selected

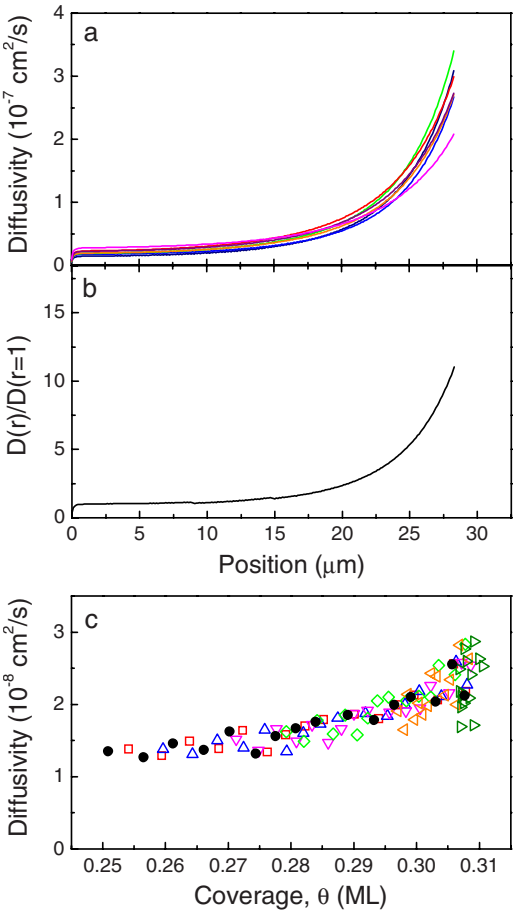

FIG. 7. (Color online) Results from the inverse solution method are shown for (a) the position and coverage-dependent diffusion coefficient $D(r,\theta)=D_0f(r)g(\theta)$ at 11 s time intervals between $t=0$ and 66 s during profile evolution, (b) the ratio of the spatial component of the diffusion coefficient $f(r)/f(r=1\ \mu\text{m})$, and (c) the coverage-dependent diffusivity $D_0[f(r=1)/f(r)]g(\theta)$ at $r=1$ (●), 3 (□), 5 (△), 8 (▽), 10 (◇), 15 (◁), and 25 μm (▷).

radial positions. In this figure, the diffusion coefficients at different radii (open symbols) have been normalized to the values at $r=1$ μm (solid symbols). The inverse of the normalization factors for every position, representing the relative spatial dependence $D(r)/D(r=1\ \mu\text{m})=f(r)/f(r=1)$, are shown in Fig. 7(b).

The diffusion coefficient that is determined directly by the inverse method increases with increasing coverage [Fig. 7(c)], which is consistent with the trend that was reported earlier.[13,28] However, the coverage dependence that is determined here is obtained with superior coverage resolution. Note that the scatter of data points in Fig. 7(c) clearly increases at higher coverage. This is a consequence of the fact that the coverage changes that occur during profile evolution in this coverage range, i.e., at the edges of the profile at all times and at the middle of the profile at late times, are small and are therefore more susceptible to noise. This demonstrates the sensitivity of the inverse solution method to noise.

The spatial dependence of the diffusion coefficient that is determined by the inverse method [Fig. 7(b)] also resembles closely the best fit of the Boltzmann functional form that was

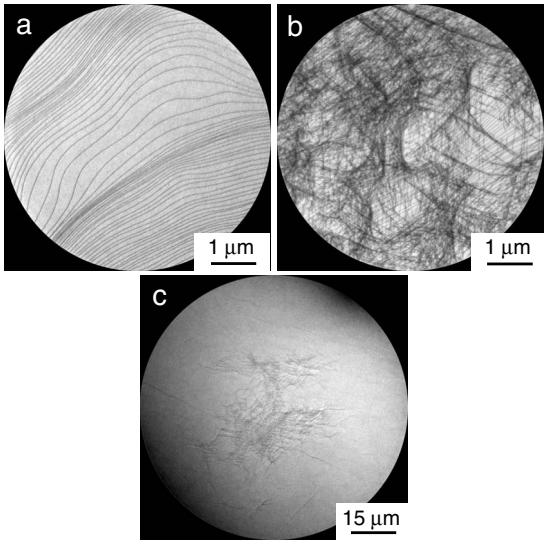

FIG. 8. LEEM images of (a) a typical region on a clean Pt(111) surface following sample preparation, (b) laser beam damage at the core of the desorption region following LITD, and (c) same as (b) with larger field of view.

assumed in the application of the predictive solution method [Fig. 6(c)]. Note that Figs. 6(c) and 7(b) have been scaled by the same factor relative to the values of the plotted quantities at $r=1$ μm. Therefore, the shapes and amplitudes of the plotted curves can be compared directly. In fact, the Boltzmann form was chosen *a posteriori* to simulate the spatial dependence that was determined by the inverse method. This produced a result for profile evolution [Fig. 6(b)] by predictive modeling that was a little better than the result that was obtained using our original uninformed choice of a Gaussian spatial form.

D. Surface morphology

Evidence of laser-induced damage that may be responsible for the spatial dependence of the diffusion coefficient is obtained directly with LEEM. Figure 8(a) shows a typical region on the surface following sample preparation. Uniform terraces with well-defined step contrast and without step pinning due to impurities are observed within the 6 μm field of view of this image. In contrast, a very high defect density is observed following LITD [Figs. 8(b) and 8(c)]. Figure 8(b) shows this damage in some details within a 6 μm field of view in the core of the desorption region. In a larger 90 μm field of view image, Fig. 8(c), the spatial extent of the damage can be seen but with some loss of the minute details of the damage that are seen so clearly in the smaller field of view image in Fig. 8(b). Although the coarse damage features do not have the ideal circular symmetry that is implied by the analysis, the spatial extent of the damaged region is comparable to the region of slow diffusion determined by the analysis of profile evolution [Figs. 6(c) and 7(b)].

III. DISCUSSION

These investigations clearly show that CO diffusion on the Pt(111) surface is hindered by the surface damage that is produced by LITD. Although it is difficult to clarify the nature of the damage that is seen in LEEM images, some isolated features in LEEM images with small field of view, such as Fig. 8(b), closely resemble atomic surface steps. These can be produced by defects in the near surface region, e.g., slip planes, where they terminate at the surface. Thus, the hindrance of diffusion by laser-induced damage may have its origin in the known kinetic limitation to CO diffusion across atomic surface steps on Pt(111).[13,14] Alternatively, the damage may be more severe due to localized melting or the features that we interpret to be damage may actually be related to residual contamination due to reaction of the adsorbate. In the event of melting, quick recrystallization following melting could produce grains with various orientations. Such recrystallization or residual contamination should produce signatures in the diffraction pattern, such as additional diffraction spots, or in the $I(V)$ characteristics. However, no such signatures were observed.

The estimated laser-pulse energy used here for desorption, 0.4 mJ, and laser spot size at the sample, 50–100 μm, indicate an average fluence of 0.01–0.05 J/cm^2. Reported values of fluence used in previous LITD-based diffusion measurements vary considerably. In many cases, the fluences used to desorb gasses from metal surfaces, 0.02 J/cm^2 for H/Ru(100),[4] 0.025 J/cm^2 for H/Rh(111),[7] 0.01 J/cm^2 for H,CO/Cu/Ru(100),[8] and 0.025 J/cm^2 for Xe/Pt(11,11,9),[9] were similar to the value we report here. These appear to be the lower range of fluences in LITD experiments. Larger fluences were also reported, 0.05–0.1 J/cm^2 for O/Ge(100),[18] 0.15 J/cm^2 for CO_2/MgO(100),[10] 0.17 J/cm^2 for NH_3/MgO(100),[11] and 3.0 J/cm^2 for CO/Pd(111).[17] The variation may be due to actual differences in desorption thresholds or to differences or uncertainties in the estimation methods. The calculation of the fluence in our work is subject to uncertainties in our estimates of pulse energy and laser spot size. We have estimated pulse energy from measurements of power when the laser is operated in repetitive (10 ns) pulse mode at 10 Hz. Small systematic offset of the measured time-averaged power can introduce error in the single pulse energy estimation. The power measurement was performed outside of the vacuum chamber at a position in front of the focusing lens and a deflecting mirror, which have to be placed as close to the chamber window as possible. These optical elements and the vacuum chamber window introduce some attenuation. The pulse energy measurement should ideally be made at the sample position in order to obtain the most accurate result. The laser spot size was estimated by the size of the desorption region that was observed with LEEM at higher laser-pulse energy. However, the desorption region only represents the area that the laser intensity exceeds the desorption threshold. Thus, the laser spot size quoted here represents a lower limit. Detailed knowledge of the pulse energy profile is needed to determine the fluence locally where desorption occurs. Despite these uncertainties, a valuable empirical observation here is that the threshold for CO desorption exceeded the threshold for laser-induced damage. We believe that this is a consequence of the small spot size and localized heating in our experimental configuration. It is also possible that the threshold for laser damage depends on properties such as optical absorption,

energy transfer from electrons to the lattice, thermal conductivity, and elastic properties of the substrate, which are material dependent. Further experimental work is needed to clarify the susceptibility of different substrate materials to laser damage in LITD-based diffusion experiments.

Even in the absence of laser-induced damage, many atomic steps are observed in the LEEM image field of view [Fig. 8(a)]. Their presence will affect mass transport over this large length scale. It might be possible to exploit the laterally resolving LEEM measurement capability to distinguish intrinsic diffusion behavior on flat terraces from diffusion in the vicinity of steps if laser damage could be avoided. Methods to reduce surface damage or to prevent it altogether must be sought. One possibility is to enlarge the laser beam size, as in the LOD method, so that the thermal shock due to laser heating will not be concentrated in such a small area. Another possibility is to use a longer laser pulse [7] to reduce the shock created in a short time.

The choice of the Boltzmann form for the spatial dependence of diffusion, Eq. (2), in the predictive modeling method was guided by the result, Fig. 7(b), of the inverse solution method. Before obtaining insight from the inverse solution, a Gaussian functional form was originally used in the predictive modeling. The best-fit profile evolution that is obtained with the Gaussian form is similar to the result obtained using the Boltzmann form, Fig. 6(b), although it does not fit the experimental data quite as well toward the end. Similarly, the best-fit values of the diffusivity scale factor D_0 that are determined for the two spatial forms differ by about only 4%, with the larger value obtained for the Gaussian spatial form. However, the optimal Gaussian spatial dependence had a full width at half maximum exceeding 100 μm. This is unphysically large compared to the evident region of beam damage seen with LEEM in Fig. 8(c). This comparison rules out the Gaussian form, even before insight is obtained by the inverse solution method. From this we also conclude that the diffusivity scale factor D_0 that is determined by the predictive method may not be very sensitive to the precise form of the spatial function that is used. Fortunately, the inverse solution method provides the insight that is necessary for proceeding with the predictive method correctly in this respect. Although the beam damage that is seen in Fig. 8 is clearly not circularly symmetric as assumed in the analysis, its nonuniformity is not reflected strongly in the two-dimensional profile evolution in Fig. 5. This is not well understood but may be a question of image noise, which is acknowledged to degrade the sensitivity to coverage variations. Nevertheless, the average spatial extent of damage is comparable to the size of the desorption region (Fig. 5) and the region of slow diffusion determined by the analyses [Figs. 6(c) and 7(b)]. It is expected that with further improvements, possibly using higher spatial resolution imaging at smaller image field of view, the current approach may be able to exploit the full two-dimensional information available in the LEEM image to resolve this issue.

These investigations have also confirmed the approximate linear coverage dependence of CO diffusion on Pt(111) in a narrower coverage range than was reported on earlier.[13,28] Figure 7(c) even shows that the enhancement of CO diffusivity with increasing coverage may even be slightly nonlinear, although the magnitude of this effect is comparable to the experimental uncertainty. Further refinements of the technique, such as the use of different signal-averaging schemes to reduce noise or the examination of stronger coverage gradients, may reveal such nonlinear effects more clearly in the future.

IV. CONCLUSIONS

The high sensitivity of LEEM to CO coverage variations on the Pt(111) surface has been determined quantitatively during adsorption. This sensitivity is used to characterize coverage profiles that are prepared by laser-induced thermal desorption and to monitor the relaxation of these nonequilibrium profiles to uniform equilibrium coverage distribution. Real-time LEEM observations of nonequilibrium profile evolution are exploited to study surface diffusion with high spatial resolution. The information on the spatial dependence of surface diffusion that is obtained by this method is uniquely complemented by the conventional sensitivity of LEEM imaging to surface structure and morphology. Alternative approaches to the data analysis that use predictive modeling and inverse solution methods show consistently and in quantitative detail that diffusion is hindered in regions that experience laser-induced surface damage. The coverage dependence of surface diffusion has also been determined by the inverse method with very high coverage resolution. The value of the inverse solution method, in general, is that it provides information that can serve as a guide for the functional forms of control parameters and governing equation that are used in the traditional predictive modeling approach.

ACKNOWLEDGMENT

The authors gratefully acknowledge the Hong Kong Research Grants Council for support under Grant No. HKUST600104.

*Corresponding author: phaltman@ust.hk

[1] R. Gomer, Rep. Prog. Phys. **53**, 917 (1990).
[2] R. Viswanathan, D. R. Burgess, P. C. Stair, and E. Weltz, J. Vac. Sci. Technol. **20**, 605 (1982).
[3] S. M. George, A. M. DeSantolo, and R. B. Hall, Surf. Sci. **159**, L425 (1985).
[4] C. H. Mak, J. L. Brand, A. A. Deckert, and S. M. George, J. Chem. Phys. **85**, 1676 (1986).
[5] E. G. Seebauer and L. D. Schmidt, Chem. Phys. Lett. **123**, 129 (1986).
[6] V. J. Kwasniewski and L. D. Schmidt, Surf. Sci. **274**, 329 (1992).

[7] S. S. Mann, T. Seto, C. J. Barnes, and D. A. King, Surf. Sci. **261**, 155 (1992).
[8] D. E. Brown, D. S. Scholl, R. T. Skodje, and S. M. George, Chem. Phys. **201**, 273 (1995).
[9] O. Sneh and S. M. George, J. Chem. Phys. **101**, 3287 (1994).
[10] D. L. Meixner, D. A. Arthur, and S. M. George, Surf. Sci. **261**, 141 (1992).
[11] D. A. Arthur, D. L. Meixner, M. Boudart, and S. M. George, J. Chem. Phys. **95**, 8521 (1991).
[12] X. D. Xiao, X. D. Zhu, W. Daum, and Y. R. Shen, Phys. Rev. Lett. **66**, 2352 (1991).
[13] Jianwei Ma, Xudong Xiao, N. J. DiNardo, and M. M. T. Loy, Phys. Rev. B **58**, 4977 (1998).
[14] Jainwei Ma, Lei Cai, Xudong Xiao, and M. M. T. Loy, Surf. Sci. **425**, 131 (1999).
[15] Jianwei Ma, Xudong Xiao, and M. M. T. Loy, Surf. Sci. **436**, L661 (1999).
[16] H. H. Rotermund, S. Nettesheim, A. von Oertzen, and G. Ertl, Surf. Sci. **275**, L645 (1992).
[17] A. von Oertzen, H. H. Rotermund, and S. Nettesheim, Chem. Phys. Lett. **199**, 131 (1992).
[18] D. Morkes, M. Ondrejcek, I. Ulrych, Z. Chvoj, H. Conrad, and V. Chab, Surf. Sci. **352-354**, 607 (1996).
[19] K. L. Man, A. B. Pang, and M. S. Altman, Surf. Sci. **601**, 4669 (2007).
[20] A. B. Pang, K. L. Man, M. S. Altman, T. J. Stasevich, F. Szalma, and T. L. Einstein, Phys. Rev. B **77**, 115424 (2008).
[21] J. B. Hannon, H. Hibino, N. C. Bartelt, B. S. Swartzentruber, T. Ogino, and G. Kellogg, Nature (London) **405**, 552 (2000).
[22] H. Pfnür, M. Lindroos, and D. Menzel, Surf. Sci. **248**, 1 (1991).
[23] C. T. Campbell, G. Ertl, H. Kuipers, and J. Segner, Surf. Sci. **107**, 207 (1981).
[24] A. Cudok, H. Froitzheim, and M. Schulze, Phys. Rev. B **47**, 13682 (1993).
[25] A. Szabó, M. Kiskinova, and J. T. Yates, J. Chem. Phys. **90**, 4604 (1989).
[26] M. Kinne, T. Fuhrmann, C. M. Whelan, J. F. Zhu, J. Pantförder, M. Probst, G. Held, R. Denecke, and H.-P. Steinrück, J. Chem. Phys. **117**, 10852 (2002).
[27] J.-S. McEwen, S. H. Payne, H. J. Kreuzer, M. Kinne, R. Denecke, and H.-P. Steinrück, Surf. Sci. **545**, 47 (2003).
[28] G. Alexandrowicz, P. R. Cole, E. Y. M. Lee, H. Hedgeland, R. Ferrando, A. P. Jardine, W. Allison, and J. Ellis, J. Am. Chem. Soc. **130**, 6789 (2008).
[29] R. Lewis and R. Gomer, Nuovo Cimento, Suppl. **5**, 506 (1967).
[30] B. Poelsema, L. K. Verheij, and G. Comsa, Phys. Rev. Lett. **49**, 1731 (1982).
[31] J. E. Reutt-Robey, D. J. Doren, Y. J. Chabal, and S. B. Christman, Phys. Rev. Lett. **61**, 2778 (1988); J. Chem. Phys. **93**, 9113 (1990).
[32] H. Froitzheim and M. Schulze, Surf. Sci. **320**, 85 (1994).
[33] E. Bauer, Rep. Prog. Phys. **57**, 895 (1994).
[34] W. F. Chung and M. S. Altman, Ultramicroscopy **74**, 237 (1998).
[35] M. Kisliuk, J. Phys. Chem. Solids **3**, 95 (1957).
[36] M. Necati Özişik, *Finite Difference Methods in Heat Transfer* (CRC, Boca Raton, FL, 1994).
[37] F. Watanabe and G. Ehrlich, Surf. Sci. **295**, 183 (1993).
[38] K. Kurpisz and A. Nowak, *Inverse Thermal Problems* (Computational Mechanics, Southampton, 1995).
[39] M. Necati Özişik and H. R. B. Orlande, *Inverse Heat Transfer: Fundamentals and Applications* (Taylor & Francis, New York, 2000).